Microstructural Characterization and Electrochemical Properties of RuO_2 Thin Film Electrodes Prepared by Reactive Radio-Frequency Magnetron Sputtering

G. Battaglin,[†] V. Rigato,[‡] S. Zandolin,[‡] A. Benedetti,[§] S. Ferro,[||] L. Nanni,[||] and A. De Battisti*[,||]

I.N.F.M., Dipartimento di Chimica Fisica dell'Università, Calle Larga S. Marta 2137, 30123 Venezia, Italy, I.N.F.M., Dipartimento di Fisica dell'Università, via Marzolo 8, 35131 Padova and I.N.F.N., Laboratori Nazionali di Legnaro, via Romea 4, 35020 Legnaro, Italy, Dipartimento di Chimica Fisica dell'Università, Calle Larga S. Marta 2137, 30123 Venezia, Italy, and Dipartimento di Chimica dell'Università, via L. Borsari 46, 44100 Ferrara, Italy

Received July 10, 2003. Revised Manuscript Received November 28, 2003

Ruthenium dioxide films were prepared by radio-frequency magnetron sputtering onto Si and Ti substrates. Films of different thicknesses (100−500 nm) were synthesized at substrate temperatures of 40, 350, and 450 °C. Their composition has been studied by Rutherford backscattering spectrometry, elastic recoil detection, and ion beam nuclear reaction analysis. Scanning electron microscopy and wide-angle X-ray scattering have been used for studying the surface texture of the samples and for their microstructural characterization, respectively. The electrochemical characterization by cyclic voltammetry has shown that, despite the high physical density of the films, compared with that obtained by the thermochemical methods, they exhibit large charge-storage capacities. For the materials synthesized at 350−450 °C, an explanation of these results has been sought in specific features of the RuO_2 rutile-type cell and columnar texture of the oxide film. The much higher capacity of the films synthesized at 40 °C would be rather due to a poor sintering of the oxide phase. Study of the chlorine evolution reaction in the samples prepared at 350 and 450 °C points to a Volmer−Tafel mechanism, with a chemical desorption rate-determining step, and significant radical intermediate coverage. Films deposited at 40 °C exhibited an unsatisfactory wear resistance under the anodic polarization required for the chlorine evolution reaction investigation.

1. Introduction

Ruthenium oxide-based film electrodes are extensively used as anodes in industrial chlor-alkali cells.[1−3] In these complex materials, RuO_2 affords good electrical conductivity to the mixed-oxide films and also acts as the catalytically active component toward the chlorine evolution reaction. The role of other possible components, such as TiO_2 and SnO_2, is essentially to stabilize the electrochemical performance of the electrode, with some secondary influence on the apparent catalytic activity, too.[4,5] The preparation method of the oxide film is based on an oxidative pyrolysis of gel-like precursor salt deposits on the chosen metal support (e.g., Ti). Because of the complicated precursor path, the composition of the resulting catalyst film is further enriched with byproducts of the incomplete thermal decomposition of reactants (e.g., ref 6 and literature therein). Typically, because of the incomplete decomposition of hydrated chlorides, often used as precursors, residual chlorides, up to 5−6 at. %, can be retained in the mixed-oxide film.[7−9] Moreover, as a consequence of the incomplete combustion of organics in the precursor mixture, carbonaceous and hydrogenated species can be trapped, with molar fractions ranging between 0.1 and 0.3.[6,10,11]

In this context, identification of the influence of the main components and of changes in the parameters of the preparation on catalytic activity and service life becomes a quite complex task. A preparation based on reactive sputtering, not involving problems of precursor reactivity, could represent an interesting alternative to

[†] I.N.F.M., Dipartimento di Chimica Fisica dell'Università.
[‡] I.N.F.M., Dipartimento di Fisica dell'Università and I.N.F.N., Laboratori Nazionali di Legnaro.
[§] Dipartimento di Chimica Fisica dell'Università.
[||] Dipartimento di Chimica dell'Università.
* Corresponding author.

(1) Trasatti, S.; Lodi, G. In *Electrodes of Conductive Metallic Oxides, Part A*; Trasatti, S., Ed.; Elsevier: Amsterdam, 1980; pp 301−358.
(2) Trasatti, S.; Lodi, G. In *Electrodes of Conductive Metallic Oxides, Part B*; Trasatti, S., Ed.; Elsevier: Amsterdam, 1981; pp 521−626.
(3) Nidola, A. In *Electrodes of Conductive Metal Oxides, Part B*; Trasatti, S., Ed.;, Elsevier: Amsterdam, 1981; p 627.
(4) Novak, D. M.; Tilak, B. V.; Conway, B. E. In *Modern Aspects of Electrochemistry*, Vol. 14; Conway, B. E., Bockris, J. O'M., Eds.; Plenum Press: New York, 1982; pp 195−317.
(5) Rolewicz, J.; Comninellis, Ch.; Plattner, E.; Hinden, J. *Electrochim. Acta* **1988**, *33*, 573.
(6) De Battisti, A.; Battaglin, G.; Benedetti, A.; Kristof, J.; Liszi, J. *Chimia* **1995**, *49*, 17.
(7) Guglielmi, M.; Colombo, P.; Rigato, V.; Battaglin, G.; Boscolo, A.; De Battisti, A. *J. Electrochem. Soc.* **1993**, *139*, 1655.
(8) De Battisti, A.; Nanni, L.; Battaglin, G.; Comninellis, Ch. In *New Promising Electrochemical Systems for Rechargeable Batteries*; Barsukov, V., Beck, F., Eds.; NATO ASI Series, Kluwer Academic: Dordrecht, The Netherlands, 1996; pp 197−211.
(9) Lodi, G.; De Battisti, A.; Bordin, G.; De Asmundis, C.; Benedetti, A. *J. Electroanal. Chem.* **1990**, *277*, 139.
(10) Pizzini, S.; Buzzanca, G.; Mari, C.; Rossi, L.; Torchio, G. *Mater. Res. Bull.* **1972**, *7*, 449.
(11) Lodi, G.; Bighi, C.; De Asmundis, C. *Mater. Chem.* **1976**, *1*, 177.

10.1021/cm034610k CCC: $27.50
Published on Web 02/11/2004

the pyrolytic preparation processes. On the basis of these considerations, in this work reactive sputtering has been used for the synthesis of electrode films based on the widely investigated electrocatalyst RuO_2, to study the correlations between preparation and properties, without the interference of significant chemical impurities and under reproducible preparative conditions.

So far, the synthesis of ruthenium oxide by reactive sputtering has been mainly studied for the production of thin film resistors and electrode/diffusion barrier layers for high dielectric constant materials to be used in capacitors for very-large-scale integrated circuits.[12−26] Oxide films were mostly prepared by reactive direct-current (dc) magnetron sputtering,[12,13,26] and only a few papers reported on the preparation of RuO_2 films by reactive radio frequency (rf) sputtering, as adopted in the present work. A detailed study by Kolawa et al.[12] has shown that stoichiometric RuO_2 films can be obtained in a narrow process window, because of the slow oxidation of ruthenium. The sputtering conditions, reported in the experimental part, were selected to obtain thin films of stoichiometric composition.

The film composition was studied by Rutherford backscattering spectrometry (RBS) and elastic recoil detection (ERD). The microstructural characterization was carried out by wide-angle X-ray scattering (WAXS).

The characterization of the surface morphology of the films was performed ex situ by scanning electron microscopy (SEM) and in situ by cyclic voltammetry. In consideration of the fact that the main application of RuO_2-based electrodes is in chlorine production, the anodic oxidation of chloride ions has been studied as a model reaction, at the prepared film electrodes.

2. Experimental Section

2.1 Electrode Preparation. RuO_2 films were synthesized using reactive rf magnetron sputtering from a 2-in. Ru (99.95%) disk. Ultrapure argon (99.9999%) and oxygen (99.995%) gases, introduced through separate mass-flow controllers, were used in the synthesis. Films of different thicknesses (in the range between 100 and 500 nm) were grown at different temperatures on Si(110) and Ti substrates. For each thickness and temperature, five samples were synthesized. The sputtering conditions are listed in Table 1. The metal supports for electrochemical use were Ti cylinders (0.785 cm^2 cross-section area). One of the two basal surfaces was mechanically polished by sand paper and then by diamond pastes of differing coarseness. Samples were then rinsed with acetone, rinsed with water, immersed for a short time (about one minute) in boiling 20% aqueous oxalic acid, and finally rinsed with distilled water.

Table 1. Sputtering Conditions for RuO_2 Films

target	Ru (99.95%)
substrate	Si(100) and Ti (Johnson & Matthey, 99.9%)
target−substrate distance	155 mm
rf power	110 W
background vacuum	3×10^{-4} Pa
total pressure	1.35 Pa
O_2 in Ar + O_2	25% [27, 28]
substrate temperature	40, 350, and 450 °C
substrate bias	0 V
target dc self-bias	−350 (± 5) V
sputter rate	13 (± 1) nm/min

The thickness of the films deposited on silicon was measured by a profilometer (alpha-step, Tencor Instruments). A step was created by masking part of the substrate during deposition. On each sample, several measurements (minimum five) were made. The reproducibility was better than 10%.

2.2 Concentration Depth Profiling. Ruthenium and oxygen concentration−depth profiles were measured by 1.8 and 2.2 MeV He^+ Rutherford backscattering spectrometry (RBS).[29,30] The backscattering yield was recorded at a scattering angle of 160°; the concentration profiles were determined from a simulation of RBS spectra with the computer code RUMP.[31]

The hydrogen content of the films, after storage in air for about one month, was measured by elastic recoil detection (ERD).[29] A 2.2 MeV He^+ beam was incident onto the sample surface with an angle of 15° with respect to it. Elastically forward-scattered protons were detected at an angle of 15° with respect to the incident beam direction. Elastically scattered He^+ particles were stopped with a 9-mm thick Mylar foil placed in front of the detector.

The $^{12}C(d,p)^{13}C$ and $^{14}N(d,p)^{15}N$ nuclear reactions were used to detect carbon and nitrogen contaminants. No traces of either of these elements could be detected (the detection limit was 0.3 at. %). The microstructure of surface and fractured cross sections of films deposited onto silicon was observed by a scanning electron microscope (SEM).

2.3 X-ray Diffraction Analysis. X-ray patterns were collected using a Philips vertical goniometer connected to a highly stabilized generator. Cu Kα Ni-filtered radiation, a graphite monochromator, and a proportional counter with a pulse-height discriminator were used. The profile intensities were measured step by step (0.05° in 2θ) in several runs for a whole fixed time of 100 s.

Line-broadening analysis was carried out according to a previously described best-fitting procedure.[32,33] In particular, with the use of the Warren−Averbach (W−A) method,[34] both the average size of the crystallites and the amount of microstrains present could be calculated. To do that, the corrected Fourier transforms $A(L)$ (L is the variable in direct space), derived from the X-ray profiles, have to be known. In the

(12) Kolawa, E.; So, F. C. T.; Pan, E. T−S.; Nicolet, M. S. *Appl. Phys. Lett.* **1987**, *50*, 854.
(13) Kolawa, E.; So, F. C. T.; Flick, W.; Zhao, X.-A.; Pan, E. T−S.; Nicolet, M. S. *Thin Solid Films* **1989**, *173*, 217.
(14) Sakiyama, K.; Onishi, S.; Ishihara, K.; Orita, K.; Kajiyama, T.; Hosoda, N.; Hara, T. *J. Electrochem. Soc.* **1993**, *140*, 834.
(15) Vijay, D. P.; Desu, S. B. *J. Electrochem. Soc.* **1993**, *140*, 2640.
(16) Jia, Q. X.; Jiao, K. L.; Anderson, W. A.; Collins, F. M. *Mater. Sci. Eng.* **1993**, *B18*, 220.
(17) Jia, Q. X.; Jiao, K. L.; Anderson, W. A.; Collins, F. M. *Mater. Sci. Eng.* **1993**, *B20*, 301.
(18) Jia, Q. X.; Jiao, K. L.; Anderson, W. A. *Thin Solid Films* **1994**, *277*, 59.
(19) Takemura, K.; Sakuma, T.; Miyasaka, Y. *Appl. Phys. Lett.* **1994**, *64*, 2967.
(20) Yoshikawa, K.; Kimura, T.; Noshiro, H.; Otani, S.; Yamada, M.; Furumura, Y. *Jpn. J. Appl. Phys.* **1994**, *33*, L867.
(21) Maiwa, H.; Ichinose, N.; Okazaki, K. *Jpn. J. Appl. Phys.* **1994**, *33*, 5223.
(22) Lee, J. G.; Min, S.-K.; Choho, S. H. *Jpn. J. Appl. Phys.* **1994**, *33*, 7080.
(23) Takemura, K.; Yamamichi, S.; Lesaicherre, P.-Y.; Tokashiki, K.; Miyamoto, H.; Ono, H.; Miyasaka, Y.; Yoshida, M. *Jpn. J. Appl. Phys.* **1995**, *34*, 5224.
(24) Lee, J.-G.; Kim, Y. T.; Choho, S. H. *J. Appl. Phys.* **1995**, *77*, 5473.
(25) Al-Shareef, H. N.; Tuttle, B. A.; Warren, W. L.; Headley, T. J.; Dimos, D.; Voigt, J. A.; Nasby, R. D. *J. Appl. Phys.* **1996**, *79*, 1013.
(26) Kim, Y. T.; Lee, C. W. *J. Appl. Phys.* **1996**, *A62*, 187.
(27) Abe, Y.; Kaga, Y.; Kawamura, M.; Sasaki, K. *J. Vac. Sci. Technol. B* **2000**, *18*, 1348.
(28) Huang, J. H.; Chen, J. S. *Thin Solid Films* **2001**, *382*, 139.
(29) Tesmer, J. R., Nastasi, M., Eds. *Handbook of Modern Ion Beam Materials Analysis*; MRS: Pittsburgh, PA, 1995.
(30) Battaglin, G.; Carnera, A.; Mazzoldi, P.; Lodi, G.; Bonora, P.; Daghetti, A.; Trasatti, S. *J. Electroanal. Chem.* **1982**, *135*, 313.
(31) Doolittle, L. R. *Nucl. Instr. Meth.* **1985**, *B9*, 344.
(32) Enzo, S.; Polizzi, S.; Benedetti, A. *Z. Kristallogr.* **1985**, *170*, 275.
(33) Benedetti, A.; Fagherazzi, G.; Enzo, S.; Battagliarin, M. *J. Appl. Crystallogr.* **1988**, *21*, 543.
(34) Warren, B. E. *X-ray Diffraction*; Addison-Wesley: Reading, MA. 1969; p 264.

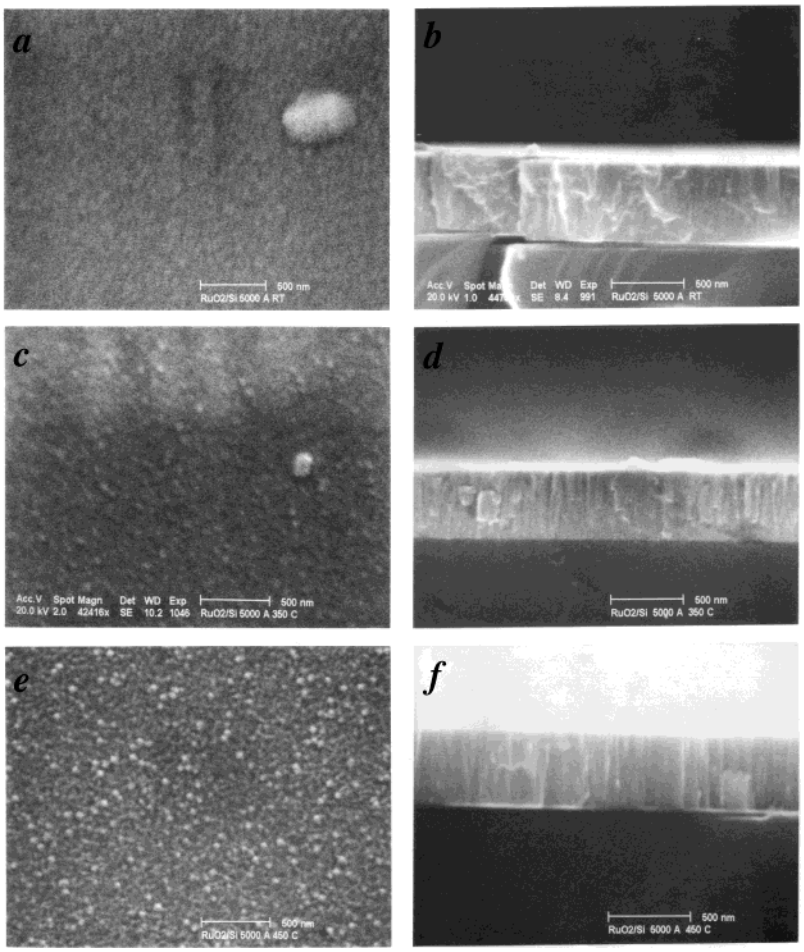

Figure 1. SEM micrographs (surface and cross-section) of 500-nm-thick samples deposited at 40, 350, and 450 °C.

analysis, each experimental crystalline peak has been fitted with two pseudo-Voigt functions, to take into account the $K_{\alpha 1}-K_{\alpha 2}$ doublet. The optimized pseudo-Voigt function, deconvoluted from the instrumental and spectral effects relating to the $K_{\alpha 1}$ component of the considered reflection, was Fourier transformed to obtain $A(L)$. If at least two orders of reflections of the same plane family are known (i.e., 110−220), it is possible to separate the crystalline size contribution from that of the lattice distortions by means of the following expression proposed by W−A:[34]

$$\ln A = \left(L, \frac{1}{d_{hkl}^2}\right) = \ln A_s(L) - 2p^2 \langle \epsilon^2(L) \rangle \frac{L^2}{d_{hkl}^2} \qquad (1)$$

where hkl are the Miller indices, $\langle \epsilon^2(L) \rangle$ is the squared microstrain averaged over all distances L, and d_{hkl} is the interplanar spacing. If only one peak for each family is known (i.e., 101, 211, and 002), all the experimental broadening was attributed to the size effect.

The volume-weighted crystalline size distribution, $p_V(L)$ has been shown to be proportional to

$$L \frac{d^2 A(L)}{dL^2} \qquad (2)$$

while the volume-weighted average crystallite size $\langle L \rangle_V$, calculated perpendicularly to the (hkl) planes, is given by

$$\langle L \rangle_V = \frac{\int L\, p_V(L) dL}{\int p_V(L) dL} \qquad (3)$$

Cell parameters were calculated by a computer refinement program, using the peak position relevant to the $K_{\alpha 1}$ monochromatic radiation obtained by the fitting procedure.

2.4 Electrochemical Measurements. Electrochemical experiments were carried out by a 1286 electrochemical interface (Solartron), in a three-electrode cell equipped with a Luggin capillary. The test solution was 1 M aqueous perchloric acid/1 M aqueous sodium perchlorate. Potentials were measured with respect to a double-walled, saturated calomel electrode (SCE), with an intermediate saturated $NaNO_3$ solution. Cyclic voltammograms were recorded in a potential window ranging from 0.10 to 1.10 V. In quasi-steady potentiostatic measurements, current was sampled at 2-mV potential intervals, recording the data after two minutes of polarization. Most of the electrochemical experiments were carried out at 500-nm thick films, as samples of other thicknesses gave essentially the same answers in terms of Tafel slope and reaction order.

3. Results and Discussion

3.1 Microstructural and Compositional Characterization. SEM pictures of the surface and cross-section of 500-nm thick films, deposited at 40, 350, and 450 °C, are shown in Figure 1a−f. No preferential growth or particle formation can be seen in the samples prepared at 40 °C. For those prepared at 350 °C, a columnar texture can be observed, which becomes more pronounced for the film prepared at 450 °C (Figure 1e). These changes of morphology in the cross-section pictures are also accompanied by an increase in the particle-like structure of the film surface (Figure 1b, d, f).

The thickness of the films seems to affect their texture, too. The 100-nm thick samples, prepared at 450

Table 2. Volume-Weighted Average Crystallite Size $\langle L \rangle_V$ Perpendicular to Different (*hkl*) Planes

deposition temperature (°C)	film thickness (nm)	W−A pair (110−220)[a] (nm)	$\langle \epsilon^2 \rangle^{1/2}$	110 (nm)	101 (nm)	210 (nm)	211 (nm)	220 (nm)
40	500	4.7		4.5			4.9	4.2
350	500	43.3	1.8×10^{-3}	36.9	49.6	29.6	30.8	23.9
450	500	40.0	1.8×10^{-3}	35.0	35.5	30.0	33.0	24.5

[a] The column labeled 110/220 shows the value corrected for contributions to the peak width due to disorder. The estimated error is of the order of 10−15%.

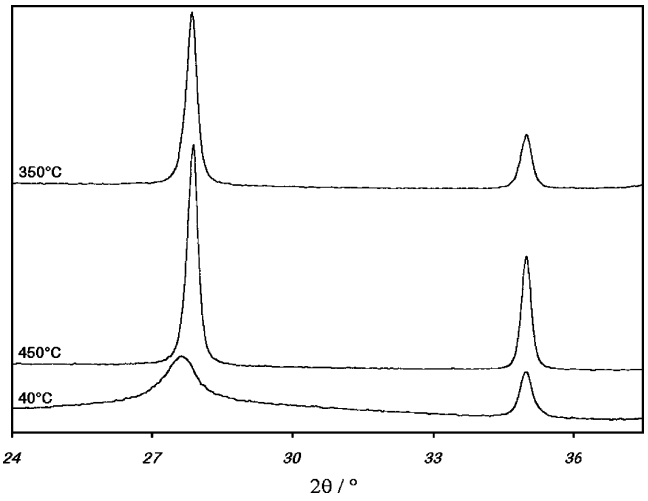

Figure 2. X-ray diffraction pattern of samples prepared at 40, 350, and 450 °C.

°C, exhibit a larger degree of macro-roughness, without any evidence of the columnar structure. The surface of the 250-nm thick films is more regular, and columnar structures appear in the 500-nm thick film. A columnar structure was also observed by Birss et al.[35] in hydrous RuO_2 films, obtained by anodic oxidation of Ruthenium metal. The similarity in the film morphology persists, despite the different growth mechanism, with reactants all in the gas phase for reactive sputtering and hydroxyl radicals progressively migrating into the Ru metal structure in the case of anodic oxide film growth.[35−37] The surface morphology characterization of the hydrous oxide films, carried out by different microscopic techniques,[35] has also detected cylindrical pores with a diameter of about 10−15 nm, absent in the films investigated in the present paper, which are necessarily more compact.

The WAXS investigation indicates that the tetragonal RuO_2 crystalline phase is present at all deposition temperatures. As shown in Figure 2, the X-ray diffraction pattern of the samples prepared at 40 °C exhibits also a halo, in the 2θ range between 20 and 70°, due to an amorphous component in the oxide film. This feature is absent in the pattern of samples deposited at higher temperatures. The results of the line broadening and of the W−A analysis are reported in Table 2. Because of the low crystallinity, in the case of the films deposited at 40 °C, only a limited number of reflections could be studied. In fact, the corresponding volume-weighted average crystallite size is smaller by about 1 order of magnitude, if compared with those obtained for the two other samples. The latter values are, however, larger than for samples prepared by sol−gel technique, after a pyrolysis at 400 °C for 20 min, in which case a $\langle L \rangle_V \approx$ 15 nm was found.[38] Under the pyrolytic preparation conditions, residual impurities from chemical reactions, like intra- and intermolecular hydrolysis and combustion of carbon compounds, probably prevent further growth of the crystallite size in the oxide phase.

Table 3. Cell Parameters and Cell Volume of RuO_2 Deposited by Reactive Sputtering, as a Function of the Deposition Temperature

temperature (°C)	thickness (nm)	cell parameters (Å) $a = b$	cell parameters (Å) c	volume (Å^3)
40	500	4.568(2)	3.100(3)	64.686
350	500	4.528(3)	3.117(3)	63.907
450	500	4.531(3)	3.110(4)	63.848
ref 39		4.490	3.106	62.617

The amount of measured microstrains, constant in the samples deposited by sputtering at 350 and 450 °C, is lower than that in samples obtained by usual sol−gel procedure (in ref 38, $\langle \epsilon \rangle^{1/2} = 6 \times 10^{-3}$). The larger size and the smaller lattice distortion witness a larger degree of order in the structure of the samples obtained by sputtering.

In the determination of cell parameters, for the samples prepared at 40 °C, only the 110, 211, and 200 reflections were utilized (for this reason, larger error on the measure is reported in Table 3). The $a_0 = b_0$ parameter of the tetragonal rutile cell is larger with respect to literature data, whereas for c_0 no significant change is observed. These different features of the cell in RuO_2 films have been observed also in preparations based on oxidative pyrolysis of $RuCl_3 \times 3H_2O$ and considered as an effect of residual chloride species in the oxide lattice[1,9−11] or a nonequilibrium state due to the film preparation method. Results of the present work would rather suggest that the phase-deposition kinetics can play an important role, causing inclusion of microstructural defects, while the role of Cl in thermochemical preparation would not be so important. The fact that a_0 values reported in Table 3 are much larger than $a_0 = 4.508(2)$, obtained for the sample prepared by thermal decomposition of the chloride-containing precursor, may serve as a further support to the above hypothesis.

Figure 3 shows the RBS spectra for RuO_2 films about 500 nm thick, deposited on silicon at temperatures of 40, 350, and 450 °C. Ruthenium and oxygen signals have been recorded, together with that of silicon from

(35) Birss, V.; Myers R.; Conway, B. E. *J. Electrochem. Soc.* **1984**, *131*, 1502.
(36) Hadzi-Jordanov, S.; Kozlowska H. A.; Conway, B. E. *J. Electroanal. Chem.* **1975**, *60*, 359.
(37) Conway, B. E. *Electrochemical Supercapacitors − Scientific Fundamentals and Technological Applications*; Kluwer Academic/Plenum Publishers: New York, 1999; pp 221−257.
(38) Nanni, L.; Polizzi, S.; Benedetti, A.; De Battisti, A. *J. Electrochem. Soc.* **1999**, *146*, 220.
(39) Joint Committee on Powder Diffraction Standards. Powder Diffraction File no. 21-1172; International Centre for Diffraction Data: Swarthmore, PA, 1988.

Table 4. Results of the Cyclic Voltammetry Characterization of the Film Electrodes

deposition temp. (°C)	film thickness (nm)	density (g cm^{-3})	anodic charge q_a (C m^{-2})	peak charge $q_{p,a}$ (C m^{-2})	roughness factor, f_R	NES[a] cm^{-2}
40	500	6.2	743.2	42.2	876.3	2.63×10^{16}
350	500	6.7	129.6	9.0	150.8	5.62×10^{15}
350	300	6.8	155.1	7.2	185.4	4.49×10^{15}
450	500	6.7	203.5	13.3	237.7	8.30×10^{15}
450	250	7.0	69.0	4.3	81.1	2.68×10^{15}
450	100	7.2	69.0	5.2	81.5	3.25×10^{15}

[a] NES = number of electroactive sites.

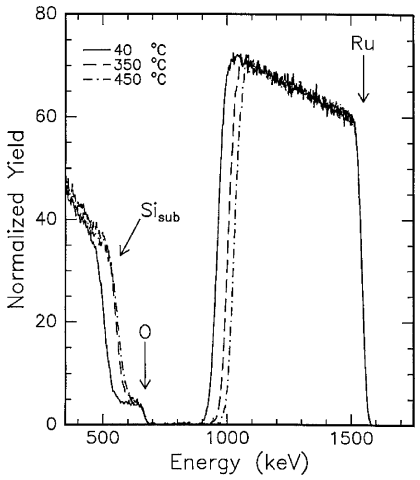

Figure 3. Ruthenium, oxygen, and silicon (from the substrate) signals in the RBS spectra for the 500-nm-thick samples deposited at 40, 350, and 450 °C. Arrows indicate the energy of particles scattered by atoms at the surface of the samples.

the substrate. By computer simulation of ruthenium and oxygen spectra, the ruthenium oxide stoichiometry was found to correspond to $RuO_{2.0\pm0.1}$ throughout the film thickness and at all deposition temperatures. These data were confirmed by the results for 100-, 250-, and 350-nm-thick samples. From the areal density of the films (obtained as at cm^{-2}, from RBS data) and profilometric results, physical densities corresponding to the literature data for bulk crystalline RuO_2 were found (Table 4), within an experimental uncertainty of about 10%. Comparison with data relative to thermally prepared RuO_2-TiO_2 films indicates, for the latter, much lower physical densities and therefore large void fraction.[7] This supports the hypothesis formulated elsewhere that pyrolytic oxidation of precursors in sol−gel or "brushing" preparation methods causes the formation of porous oxide films.[6,8]

Under the conditions described in the Experimental Section, the thickness accessible to ERD analysis for hydrogen species was 280 nm. Typical ERD spectra are shown in Figure 4 for *as-prepared* films. The distribution of the analyte across the film is nearly constant, with a slight trend to decrease with increasing depth. For the RuO_2 films synthesized at 40 °C, a hydrogen content of 0.18 ± 0.02 H atoms per RuO_2 molecule has been estimated. In samples prepared at 350 and 450 °C, the hydrogen content was 0.07 ± 0.01 H atoms per RuO_2 molecule.

After polarization at the two potential limits of the cyclic voltammogram, electrodes were rinsed with water, then rinsed with acetone, and eventually kept in a dehydrator till the transfer to the measure chamber. In these cases, ERD investigation could not detect any change in the hydrogen content, which may be taken as an indication that only the outermost part of the films is involved in a very fast proton exchange.

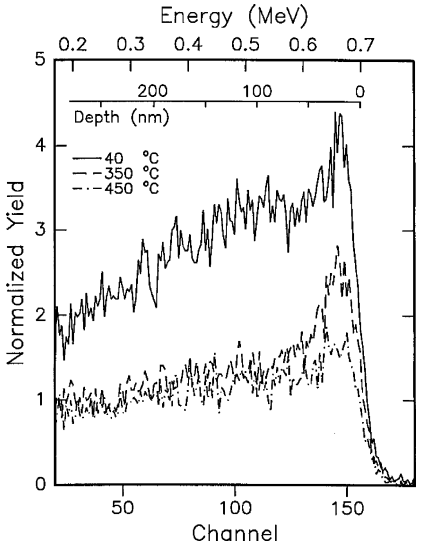

Figure 4. Hydrogen distribution profiles from ERD spectra for the *as-prepared* 500-nm-thick samples, deposited at 40, 350, and 450 °C.

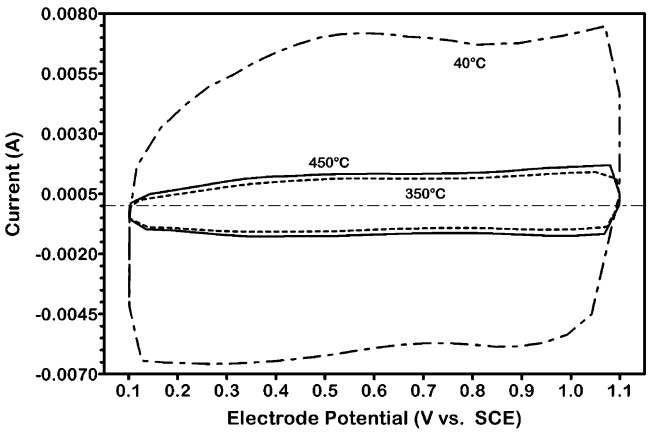

Figure 5. Cyclic voltammetry of 500-nm-thick samples deposited at 40, 350, and 450 °C, recorded in 1 M $HClO_4$/1 M $NaClO_4$ at a potential scan-rate of 0.1 V s^{-1}.

D^+ exchange experiments in thermally prepared oxide films of different composition have shown that the net uptake of counterions at potentials around 0.1 V may amount to several ions percent noble-metal ions.[40] This is in agreement with the much more porous character of thermal oxides compared with those dealt with in the present work.

3.2 Electrochemical Characterization. *3.2.1 Cyclic Voltammetry*. Typical voltammograms, obtained in 1 M $HClO_4$/1 M $NaClO_4$ at a potential scan rate *s* of 0.1 V s^{-1}, are shown in Figure 5 for the specific case of the 500-nm-thick samples synthesized at 40, 350, and 450 °C. Within each set of five samples, defined by film thickness and deposition temperature, the reproducibility of voltammetric currents was around ±5% and the shape of voltammograms was essentially the same, as shown in Figure 5. The shape in Figure 5 is also quite

(40) Battaglin, G.; De Battisti, A.; Barbieri, A.; Giatti, A.; Marchi, A. *Surf. Sci.* **1991**, *251/252*, 73.

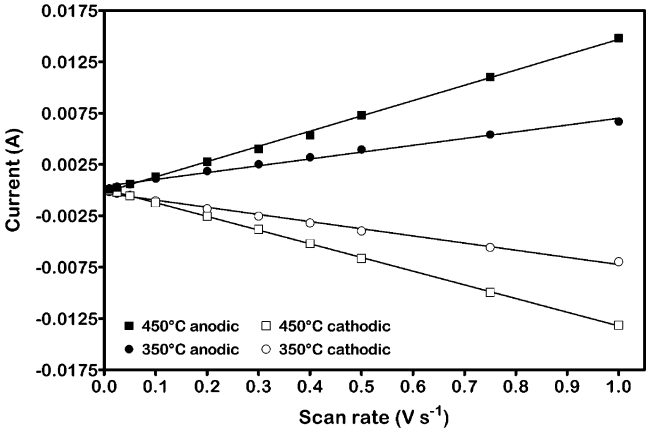

Figure 6. Dependence of the voltammetric current density, anodic and cathodic ($E = 0.70$ V, vs SCE) on the potential scan-rate, *s*, for two 500-nm film electrodes (synthesis temperatures 350 and 450 °C, respectively).

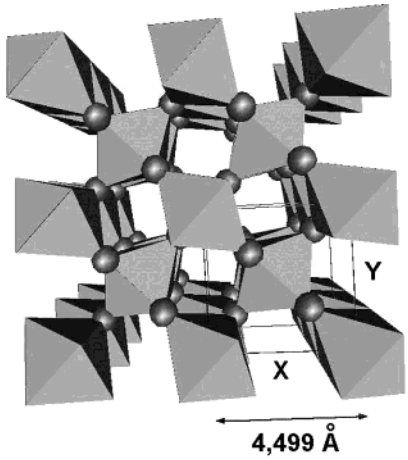

Figure 7. Schematic representation of the rutile structure of RuO_2 showing the void channels normal to the 001 plane.

similar to that of voltammograms reported in the literature for RuO_2 electrodes prepared by different methods,[1] retaining the relatively featureless character, with broad peaks in the potential region from 0.2 to 0.6 V and also significant voltammetric current values. In all the examined cases, voltammetric currents have been found to be linearly dependent on *s*, as shown in Figure 6 for the particular case of the 500-nm-thick films prepared at 350 and 450 °C. Following a procedure elsewhere applied[42,43] and bearing in mind its merely qualitative character,[37] the total anodic voltammetric charge and the peak charge, q_a and $q_{p,a}$ respectively, have been calculated, and results (averaged on five samples per thickness and temperature) are reported in Table 4. Considering the 500-nm-thick films, the increase in the deposition temperature from 40 to 350 °C causes a sharp decrease of q_a, possibly due to an improvement of the sintering process throughout the films and to the disappearance of the amorphous component. The moderate increase in q_a (from 9.4 to 14.8 mC), when the deposition temperature is further increased from 350 to 450 °C, can be attributed to some increase of macro-roughness, related to the outermost part of the columnar texture and to the enhancement of the columnar character of the film texture. The charge decrease observed at constant synthesis temperature and decreasing thickness could be tentatively explained in the same way. In fact, SEM observations indicate that the columnar structure, i.e., the appearance of well-defined particles, is hindered by the low thickness.

From the total anodic voltammetric charge and the peak charge, the nonfaradaic contribution was calculated. Making use of literature data for the capacity per effective unit area, the effective roughness factor f_R of film electrodes has been calculated, with an error ranging between 5 and 20%. Results, calculated assuming a value of 0.80 F m^{-2} for C,[41−43] are shown in Table 4.

It is interesting to observe that the f_R value of about 900 found for electrode films obtained at 40 °C is much larger than that for those deposited at 350 and 450 °C. This very high value can be tentatively related to the important amorphous-nanocrystalline component of the oxide phase formed under low-temperature deposition conditions, as witnessed by the previously mentioned halos in XRD spectra (Figure 2). On an essentially qualitative basis, both the average crystallite size below WAXS detection limits and the observed larger elementary cell expansion can justify a generalized facilitation of charge storage. Some role can be played also by a poorer sintering of the oxide films synthesized at the lower temperature, reflected by the scarce wear-resistance of the latter, particularly observable during quasi-steady polarization experiments.

However, all other coatings prepared at 350 and 450 °C exhibit roughness factors that are comparable with those of RuO_2 films prepared by traditional thermal decomposition methods, although their thickness is never higher than 500 nm and therefore much lower than those of thermally prepared films (about 1 μm thick). Even the samples synthesized at 450 °C, with the lowest thickness (100 nm), maintain a roughness factor of about 82. According to the above results, although the "void fraction" in the oxide films is small, if any, the apparent roughness factor remains comparable with that of less dense thermally prepared films. Properties more intrinsic to the oxide phase structure could then play some role. In fact, void channels exist in the rutile structure, with square-section channels normal to the 001 plane being present, as shown in Figure 7. Migration of smaller charged particles, such as protons, could then allow larger charge storage. Considering that the microstructural features, as determined by X-ray diffraction, do not exhibit significant dependence on the thermal treatment, the observed electrochemical properties could rather be explained taking into consideration the columnar texture shown by SEM micrographs (Figure 1a−f), which is more pronounced at higher temperatures. In this case, the border-region along the columnar texture elements could contribute to the charge-storage capacity. The free space associated with these regions, however, seems to be small enough not to influence the apparent density of the coatings and to account for the whole anomalous effect. On the basis of the above considerations, a combination of the two factors could be a more satisfactory

(41) Siviglia, P.; Daghetti, A.; Trasatti, S. *Colloids Surf.* **1982**, *7*, 15.
(42) Benedetti, A.; Riello, P.; Battaglin, G.; De Battisti, A.; Barbieri, A. *J. Electroanal. Chem.* **1994**, *376*, 195.
(43) Daolio, S.; Facchin, B.; Pagura, C.; De Battisti, A.; Barbieri A.; Kristof, J. *J. Mater. Chem.* **1994**, *4*, 1255.

explanation of voltammetric results. The void channels inside the structure could better play their role when the space along the columns becomes accessible. Accordingly, larger film thickness and higher deposition temperature should favor a better organization of the solid phase and therefore larger capacity, which is in agreement with the experimental data in Table 4. Along these lines, the charging process of the RuO_2 surface should be assisted by migration of protons at the extent allowed by the presence of structural channels. In this respect, the distinction of faradaic and nonfaradaic component of the oxide film charging becomes somewhat less clear-cut.

Making use of peak charges, the number of electroactive sites has been estimated.[42,43] As shown in Table 4, the value of 2.63×10^{16} cm^{-2} for the sample synthesized at 40 °C is quite high. However, this parameter remains high also for the more stable samples prepared at higher temperatures, ranging between a maximum of about 8×10^{15} and a minimum of about 3×10^{15} cm^{-2}. This implies a significant extension of the charging process to the near-surface region of the films. Considering the interpretation of the voltammetric behavior of RuO_2 given by Conway,[37] the above values would be rather an under-estimation of the effective number of sites capable of undergoing oxidation state changes in the film.

3.2.2 Chlorine Evolution Reaction. For the study of the chlorine evolution reaction (ChlER), quasi-steady polarization experiments have been carried out, prepolarizing the electrodes at a potential of 1.45 V before starting the polarization curve. Tafel slopes, recorded at electrodes 500-nm thick and prepared at 350 and 450 °C, were 46.7 and 46.9 mV, respectively, and related reaction orders with respect to Cl^-, R_{Cl}, were 1.35 and 1.43. Despite the relatively "facile" character of the ChlER, many mechanisms have been proposed, but, at the present level of our investigation, we will consider the two simpler schemes: the Volmer−Tafel (chemical desorption mechanism) and the Volmer−Heyrovsky (electrochemical desorption mechanism). Assuming very low values of coverage by the adsorbed Cl radical, the above-reported Tafel slopes would support the idea of an electrochemical desorption as rate determining step (rds). However, the reaction order is much lower than the expected value of 2. The alternative assumption of the chemical desorption as rds would imply a Tafel slope of 30 mV and again $R_{Cl} = 2$.

Conway et al.[44] have discussed the influence of the coverage of adsorbed intermediates on Tafel slope and reaction order. Following their approach, and with the assumption of a Langmuirian behavior of adsorbed chloro-radicals, we have $b_{app} = b_{real}/(1 - \theta_{Cl})$, whereas for the reaction order we have $(R_{Cl})_{app} = (R_{Cl})_{real} \times (1 - \theta_{Cl})$. Making use of these relations and of the b and R_{Cl} values found in the present work, a θ_{Cl} value of 0.36 can be hypothesized. A chemical desorption mechanism, coupled with a significant coverage by chloro-radicals, seems therefore the most probable, at this stage of the work.

The rate of the ChlER is higher at the film electrodes prepared at 450 °C. As previously discussed, these electrodes have also the larger capacitive and peak charges. The capacitive charge is about 1.58 times that of the samples prepared at 350 °C, whereas the ratio between the two peak charges is 1.48. Considering that the ratio between the chlorine evolution currents, at constant potential in the Tafel region, is about 3, the macro-roughness of the electrode surface seems to affect the chlorine evolution reaction in a quite straightforward way.

4. Conclusions

As discussed in the Introduction, the preparation of oxide electrocatalysts by the traditional methods based on oxidative pyrolysis of suitable precursors involves the incorporation of chemical impurities. Release of CO_2, H_2O, HCl, and Cl_2 during the thermal decomposition process is expected to make the oxide films very porous. These factors, difficult to control and reproduce, may mask important properties intrinsic to the different oxide components.

Results of the present work allow interesting conclusions. Regarding microstructural properties of ruthenium oxide, it has been shown that distortion of the cell parameters is observed also in the absence of chemical impurity incorporation as interstitial chloride or hydroxyl ions.

Another important point is the voltammetric charge of film electrodes, which is substantially as high as that of thermally prepared oxides. Apparently, the contribution to the roughness factor, due to the features of the precursor reactions, does not seem to be so important. A possible explanation of the intrinsically high charge-storage capacity of pure crystalline ruthenium oxide may be sought in the possibility of counterion (proton) migration along both void channels in the rutile structure of the oxide and border regions along the columnar texture.

Data on the ChlER differ from those found for thermally prepared oxides. Reaction orders from 1.35 to 1.43 are found, whereas for thermally prepared RuO_2-based film electrodes values much closer to 1 are typically met. These values, together with Tafel slopes of about 47 mV, allow an interpretation of the mechanism in terms of a Volmer−Tafel mechanism, with a relatively high coverage by adsorbed Cl radicals ($\theta_{Cl} = 0.2-0.4$). At RuO_2 films prepared by reactive sputtering the chlorine evolution reaction seems to be interpretable by the simplest mechanisms, with the absence of porosity in the films eliminating some of the contradictory results obtained at thermal oxides.[2] Further work is needed to supply further experimental evidence on the subject.

(44) Conway, B. E.; Tilak, B. V. *Electrochim. Acta* **1992**, *37*, 51.

CM034610K